Multiphase SPH Simulation for Interactive Fluids and Solids

Xiao Yan
Tsinghua University

Yun-Tao Jiang
Tsinghua University

Chen-Feng Li
Swansea University

Ralph R. Martin
Cardiff University

Shi-Min Hu*
Tsinghua University

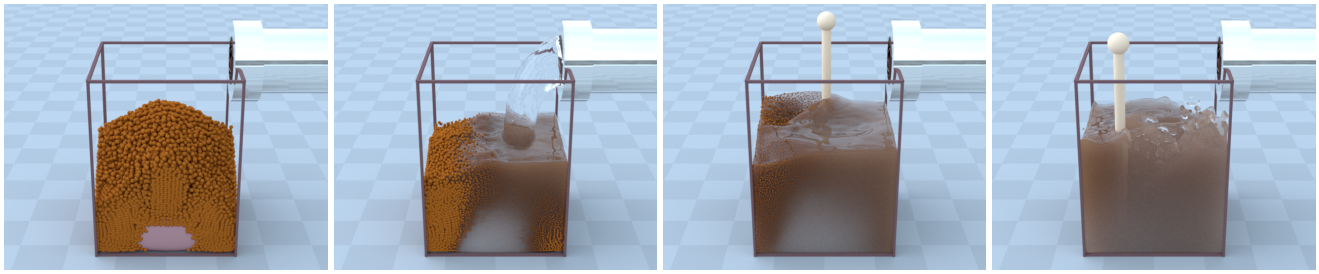

Figure 1: *Instant coffee and a soft candy dissolving in water.*

Abstract

This work extends existing multiphase-fluid SPH frameworks to cover solid phases, including deformable bodies and granular materials. In our extended multiphase SPH framework, the distribution and shapes of all phases, both fluids and solids, are uniformly represented by their volume fraction functions. The dynamics of the multiphase system is governed by conservation of mass and momentum within different phases. The behavior of individual phases and the interactions between them are represented by corresponding constitutive laws, which are functions of the volume fraction fields and the velocity fields. Our generalized multiphase SPH framework does not require separate equations for specific phases or tedious interface tracking. As the distribution, shape and motion of each phase is represented and resolved in the same way, the proposed approach is robust, efficient and easy to implement. Various simulation results are presented to demonstrate the capabilities of our new multiphase SPH framework, including deformable bodies, granular materials, interaction between multiple fluids and deformable solids, flow in porous media, and dissolution of deformable solids.

Keywords: smoothed particle hydrodynamics (SPH), fluid-solid interaction, multiphase flow, deformable bodies, granular materials

Concepts: •**Computing methodologies** → *Physical simulation;*

1 Introduction

Animations involving fluids and solids have recently become ever more popular in computer graphics, leading to the development of various physically based simulation methods, either grid-based or particle-based. The most popular particle-based approaches rely on smoothed particle hydrodynamics (SPH) [Monaghan 1992], which was first introduced into the graphics community by Müller et al. [2003] to simulate fluid flow. The SPH method has also been used to simulate elastoplastic solids [Müller et al. 2004; Gerszewski et al. 2009], and granular materials like sand [Alduán and Otaduy 2011]. Fluid-solid coupling has also been achieved within the SPH framework, to simulate fluid interacting with an elastoplastic solid [Solenthaler et al. 2007; Keiser et al. 2005], fluid interacting with granular materials [Lenaerts and Dutr 2009], and porous materials [Lenaerts et al. 2008].

More recently, by introducing the concept of volume fraction, the standard SPH method was extended to simulate multiphase flow [Ren et al. 2014; Yang et al. 2015], using a mixture model and Helmholtz free energy. A wide range of multiphase flow phenomena with rich visual effects were captured, including mixing, unmixing and extraction effects. Despite the impressive results, the multiphase-fluid SPH framework can only model fluid flows and the interactions between different fluids. It is possible to couple the multiphase-fluid SPH framework with existing SPH solid simulators [Müller et al. 2004; Gerszewski et al. 2009; Zhu and Bridson 2005; Alduán and Otaduy 2011]. However, as the multiphase-fluid SPH framework differs from the standard SPH method both in the underlying variables and in the governing equations, a naive coupling strategy requires major changes to be made to both fluid and solid simulators. Different coupling schemes are needed for specific multiphase fluid-solid interactions, making the task both messy and problem-specific.

In this work we extend the multiphase-fluid SPH framework proposed by [Ren et al. 2014; Yang et al. 2015] to cover solid phases, including both deformable bodies and granular materials. Specifically, the distributions of all phases (fluids and solids) in the simulation domain are represented by their volume fraction functions. The dynamics of the multiphase system are governed by the conservation of mass and momentum within different phases. The constitutive laws for different phases are all defined in the same form as functions of the velocity fields. The interactions between different phases are implicitly modelled in the constitutive laws which are functions of the volume fraction fields. Our main contributions are thus fourfold:

1. By extending the previous multiphase-fluid SPH framework to incorporate solid phases, a truly multiphase SPH framework is established, which supports the simulation of fluids, deformable bodies, granular materials, etc.

2. The distribution and behaviour of all phases are modelled in the same way using the same set of variables and the same

*Corresponding author. E-mail:shimin@tsinghua.edu.cn

SIGGRAPH '16 Technical Paper,, July 24-28, 2016, Anaheim, CA,
ISBN: 978-1-4503-4279-7/16/07
DOI: http://dx.doi.org/10.1145/2897824.2925897

form of governing equations, which greatly reduces the computational and implementation complexity.

3. A new way of modelling fluid-solid interaction (FSI) is established: the interactions between different phases are uniformly modelled via the multiphase constitutive laws, which are functions of volume fraction fields. This new FSI model readily scales as more phases are added to the multiphase system.

4. A much wider range of fluid-solid phenomena can be captured by this extended multiphase SPH framework, including miscible and immiscible solids and fluids, fluid-solid interaction, solid dissolution, porous media flow, etc.

2 Related Work

The area of physically based simulation has considered fluid, solid and granular material simulation. Some work can handle the couplings and interactions between different kinds of materials. Our work extends particle-based multiphase-fluid simulation to consider both solids and granular materials as well as the interactions between solids and fluids. We thus summarise previous work on these topics and to keep the review short and most relevant to the current work, we focus mainly on particle-based methods.

Particle-based Fluid Simulation: Particle-based methods are often used for fluid simulation in computer graphics, among which SPH methods are the most popular approach. Müller et al. [2003] proposed a particle-based method based on the SPH framework to simulate liquids. Becker and Teschner [2007] changed the equation of state used in SPH to achieve weakly compressible fluid effects. Solenthaler and Pajarola [2009] and Ihmsen et al. [2014a] used iteration to predict the density of particles at the next step to simulate incompressible fluids. In an alternative approach to Lagrangian-based fluid simulation, position based fluids (PBF) Macklin et al.[2013] use constrained particle positions; GPU implementations provide real-time simulation. Such work has developed the capabilities of Lagrangian-based fluid simulation in computer graphics, but does little to consider multiphase-fluid simulation.

Solids and Granular Material: To simulate deformable solids, Müller et al. [2004] proposed a particle based method using Green-Saint-Venant strain to determine the stress tensor. The method stores positions of the original neighbouring particles in order to calculate strain in deformable solids. Gerszewski et al. [2009] proposed a new method for calculating the deformation gradient based on approximating the affine transformation between the original structure and the current structure. Becker et al. [2009] gave a corotational approach based on calculating nodal rotations. Zhou et al. [2013] extended Gerszewski's work to use implicit integration. Müller et al. [2005a] used shape matching methods to simulate deformable objects, and the work was later extended by using oriented particles to simulate various 2D and 3D objects [Müller and Chentanez 2011]. Jones et al. [2014] presented a point-based approach for animating elastoplastic materials, where an "embedded space" was used to achieve more accurate estimation of large plastic deformation. In the past two decades, the material point method (MPM) archived advanced development for various materials simulations. As a particle-in-cell method, the MPM can handle history-dependent materials which are difficult to model using pure Eulerian methods, and it can also prevent the distortion that often arise in Lagrangian approaches [Sulsky et al. 1994]. In the area of computer graphics, Stomakin et al.[2013] used MPM for simulating snow, and then combined the framework of FLIP to simulate heat transport, melting and solidifying materials [Stomakhin et al. 2014].

To simulate granular materials such as sand and grain, Zhu and Bridson [2005] proposed a simplified method in which the spatial domain is decomposed into a rigid body domain and a shear flow domain. Bell et al. [2005] simulate granular material by considering the normal and shear forces on each particle. Alduán and Otaduy [2011] proposed an approach which constrains the strain rate according to the friction force, and applied a cohesion model based on the Drucker-Prager criterion in a PCISPH framework. Narain et al. [2010] combined grid and particle methods to couple sand and a rigid body. Ihmsen et al. [2012] simulated granular materials using two size scales to achieve high resolution sand simulations.

These particle-based simulation schemes are effective for the specific solid materials that are targeted, but they cannot be easily extended to cope with fluid flow, especially multiphase fluids.

Fluid-solid Coupling and Interaction Keiser et al. [2005] simulated fluid flow with deformable solids in a unified Naive-Stocks equation framework, which supports phase transition. Solenthaler et al. [2007] extended previous SPH-based solid and fluid frameworks to handle a wider range of phenomena such as solidification and melting. Lenaerts et al.[2008] proposed a coupling method for porous materials and fluids, which was later extended by Lenaerts and Dutr [2009] to simulate sand and water coupling. Akinci et al. [2012] proposed a novel method for coupling fluids with rigid bodies which used boundary particle volume correction and friction forces; they later extended it to resolve the coupling between fluid and elastic solid [Akinci et al. 2013]. Shao et al. [2015] combined lattice shape matching method and PCISPH to model coupling between fluids and solids.

In all these research, the particles can only be determined as pure fluid or pure solid. Hence, they can only handle immiscible fluid and solid and cannot simulate continuous transition processes such as dissolution. Also, none of these methods considered multiphase fluids in the simulation framework.

SPH based Multiphase Fluids Ren et al. [2014] introduced the concept of volume fraction into SPH fluid simulation and developed a multiphase-fluid SPH scheme using the mixture model. Their method allows the simulation of a wide range of multiphase flow phenomena, such as mixing and unmixing etc. This approach was later extended [Yang et al. 2015] by using Helmholtz free energy to enable extraction and phase control in a multiphase fluid system. However, the multiphase-fluid SPH approach is designed for fluid simulation only, and does not handle solid phases. Also, as the underlying variables and governing equations are different from the standard SPH method, the multiphase fluid SPH framework cannot be easily coupled with existing SPH schemes for solids.

This work aims to extend the existing multiphase-fluid SPH framework to cover solid phases, and build a truly multiphase SPH scheme, handling both fluids and solids. The main challenges are: 1) how to efficiently represent the distribution and shape of all phases with the least computational and implementation complexity; 2) how to resolve the behaviour of different phases without adding separate equations for each specific phase; 3) how to take into account the interactions between multiple fluid and solid phases.

3 Multiphase SPH simulation

Our method is based on SPH methods which are often used in fluid simulation since they are simple and effective. By introducing the mixture deviatoric stress tensor into the mixture model momentum equation, we extend the multiphase-fluid SPH framework

[Ren et al. 2014] for simulating the interaction between fluids and solids. We now briefly introduce the foundations of our approach.

SPH Fluid Simulation

Smoothed particle hydrodynamics, or SPH, is a Lagrangian based simulation method which discretizes and samples the spatial domain containing fluid by means of particles having position $\boldsymbol{x}$, rest density ρ_0, mass m, and other properties. Continuous properties can be estimated by interpolation between the property values at particles surrounding a point [Monaghan 1992; Ihmsen et al. 2014b] using the following formula:

$$A(\boldsymbol{x}) = \sum_j \frac{m_j A_j}{\rho_j} W_{ij}(\boldsymbol{x}_i - \boldsymbol{x}_j, h),$$

where $A(\boldsymbol{x})$ is some continuous variable such as density or inertial force, A_j is its value at particle j, m_j is the mass of particle j, ρ_j is particle density, W_{ij} is a symmetric kernel function, h is the smoothing radius and $\boldsymbol{x}_j$ is the position of particle j; j runs over the nearby particles.

Spatial derivatives at a particle can be approximated using:

$$\nabla A_i = \rho_i \sum_j m_j \left(\frac{A_i}{\rho_i^2} + \frac{A_j}{\rho_j^2} \right) \nabla W_{ij}(\boldsymbol{x}_i - \boldsymbol{x}_j, h),$$
$$\nabla \cdot \boldsymbol{A}_i = -\frac{1}{\rho_i} \sum_j m_j (\boldsymbol{A}_j \pm \boldsymbol{A}_i) \cdot \nabla W_{ij}(\boldsymbol{x}_i - \boldsymbol{x}_j, h).$$

The pressure at a particle is calculated from the state equation:

$$p_i = k_s(\rho_i - \rho_0) \tag{1}$$

where k_s is the stiffness coefficient related to the bulk modulus.

An alternative state equation for weakly compressible fluids is Becker et al. [2007]:

$$p_i = k_s \left((\rho_i/\rho_0)^7 - 1 \right). \tag{2}$$

To compute the pressure force on an SPH particle, the following equation is typically used:

$$\boldsymbol{F}_i^p = -m_i \sum_j m_j \left(\frac{p_i}{\rho_i^2} + \frac{p_j}{\rho_j^2} \right) \nabla W_{ij}, \tag{3}$$

where $\boldsymbol{F}_i^p$ is the pressure force on particle i due to the the surrounding particles.

Multiphase-fluid SPH Simulation By introducing the concept of volume fraction into the standard SPH scheme, a multiphase-fluid SPH framework was proposed in [Ren et al. 2014; Yang et al. 2015] to simulate various multiphase flow phenomena, where the mixing and unmixing effects are handled via a mixture model and Helmholtz free energy. We use the mixture model presented in [Ren et al. 2014] and extend it to also allow simulation of solids and their interaction with fluids. The formulation of the mixture model is briefly introduced here, and the reader is referred to the original paper for details.

The continuity equation in the mixture model is:

$$\frac{\mathrm{D}\rho_m}{\mathrm{D}t} = \frac{\partial \rho_m}{\partial t} + \nabla \cdot (\rho_m \boldsymbol{u}_m) = 0$$

where $\boldsymbol{u}_m$ is the mass-averaged mixture velocity, averaged over all phases:

$$\boldsymbol{u}_m = \sum_{k=1}^{n} c_k \boldsymbol{u}_k.$$

Here, c_k is the mass fraction: $c_k = \alpha_k \rho_k / \rho_m$ where α_k is the volume fraction for phase k and n is the number of different phases; ρ_m is the rest density of the mixture:

$$\rho_m = \sum_{k=1}^{n} \alpha_k \rho_k,$$

where ρ_k is the rest density of a single phase.

The momentum equation for the mixture can be expressed as:

$$\frac{\mathrm{D}(\rho_m \boldsymbol{u}_m)}{\mathrm{D}t} = -\nabla p + \nabla \cdot (\boldsymbol{\tau}_m + \boldsymbol{\tau}_{Dm}) + \rho_m \boldsymbol{g} \tag{4}$$

where $\boldsymbol{\tau}_m$ is the viscous stress tensor, $\boldsymbol{\tau}_{Dm}$ is the diffusion tensor and $\boldsymbol{g}$ is the overall external body force, e.g. due to gravity.

At each time step, the model calculates the drift velocity $\boldsymbol{u}_{mk}$ which is defined as the relative velocity of phase k to the mixture, i.e. $\boldsymbol{u}_{mk} = \boldsymbol{u}_k - \boldsymbol{u}_m$. In full, the drift velocity is given by:

$$\begin{aligned} \boldsymbol{u}_{mk} = {} & \nu_k \left(\rho_k - \sum_{k'} c_{k'} \rho_{k'} \right) \boldsymbol{a} - \\ & \nu_k \left(\nabla p_k - \sum_{k'} c_{k'} \nabla p_{k'} \right) - \mu_k \left(\frac{\nabla \alpha_k}{\alpha_k} - \sum_{k'} c_{k'} \frac{\nabla \alpha_{k'}}{\alpha_{k'}} \right) \end{aligned} \tag{5}$$

where $\boldsymbol{a} = \boldsymbol{g} - (\boldsymbol{u}_m \cdot \nabla)\boldsymbol{u}_m - \partial \boldsymbol{u}_m / \partial t$. The first term on the right hand side represents the slip velocity due to body forces (e.g. gravity and centrifugal force). The second term represents the pressure effect that causes the fluid phases to move from high pressure regions to low pressure regions. The third term represents Brownian diffusion, i.e. the fluid phases drifting from high concentration regions to low concentration regions. The parameter ν is the coefficient of diffusion due to the slip and pressure gradient, and μ is the Brownian diffusion coefficient.

The drift velocity $\boldsymbol{u}_{mk}$ is used to calculate the diffusion tensor and advect the volume fraction as below:

$$\boldsymbol{\tau}_{Dm} = -\sum_k \alpha_k \rho_k \boldsymbol{u}_{mk} \otimes \boldsymbol{u}_{mk} \tag{6}$$

$$\frac{\mathrm{D}\alpha_k}{\mathrm{D}t} = -\alpha_k \nabla \cdot \boldsymbol{u}_m - \nabla \cdot (\alpha_k \boldsymbol{u}_{mk}) \tag{7}$$

where $\otimes$ denotes the tensor product.

The implementation of the mixture model is summarized in Algorithm 1.

Algorithm 1 Implementation of the multiple-fluid mixture model

repeat
  for each particle i **do**
    compute the density and the pressure for each particle using standard SPH.
  end for
  for each particle i **do**
    compute the drift velocity using Eqn. (5), then compute the diffusion tensor and correct α using Eqn. (6) and Eqn. (7).
  end for
  for each particle i **do**
    compute the total force acting on the particle and advance the particle.
  end for
  $t \leftarrow t + \Delta t$
until end of simulation

Extensions to Handle Solids In order to extend the original multiphase-fluid approach to solids, we need to change the momentum equation of multiphase flow. Multiphase flow simulation needs the pressure to be continuous at the interface between phases to ensure consistent pressure forces [Solenthaler and Pajarola 2008]. We thus retain and solve the pressure term ∇p for both fluid and solid phases and treat the shear stress in deformable solids in a similar way to the viscosity tensor term. Specifically, an extra internal deviatoric stress tensor is added to the right hand side of Eqn.(4) to handle solids in the multiphase simulation. The momentum equation Eqn.(4) now becomes:

$$\frac{\mathrm{D}(\rho_m \boldsymbol{u}_m)}{\mathrm{D}t} = -\nabla p + \nabla \cdot (\boldsymbol{\tau}_{Sm} + \boldsymbol{\tau}_m + \boldsymbol{\tau}_{Dm}) + \rho_m \boldsymbol{g} \quad (8)$$

where $\boldsymbol{\tau}_{Sm}$ is the mixture deviatoric stress tensor, which depends on the deviatoric stress tensor of the solid phase, i.e. the constitutive law of the solid. Two types of constitutive laws are considered in this work for the solid phase: the elastoplastic law for modelling deformable bodies and the hypoplastic law for modelling granular materials, which are explained in Section 4. We use strain rate to calculate the stress in elastoplastic materials via a simplified model; as it only depends on the velocity gradient, it is easy to incorporate into our multiphase framework. A hypoplastic model is often used to simulate granular materials, and again only depends on the velocity gradient.

In Section 5, we describe how to discretize Eqn. (8) for both miscible phases and immiscible phases in a unified framework following previous multiphase-fluid framework, allowing us to simulate various phenomena such as interactions of miscible and immiscible phases, and dissolution effects.

4 Constitutive Laws of Solid Materials

Section 3 discussed use of a deviatoric stress tensor which depends on the constitutive law of a solid material. Here, we describe the constitutive laws for two types of solids: elastoplastic materials, such as chewing gum, and hypoplastic materials, such as a pile of sand or granules.

To simplify the following, we define a function $\mathscr{D}$ operating on any tensor $\boldsymbol{\tau}$ to give its deviatoric part:

$$\mathscr{D}(\boldsymbol{\tau}) := \boldsymbol{\tau} - \frac{1}{3}\mathrm{Tr}(\boldsymbol{\tau})\boldsymbol{I}.$$

Thus, the deviatoric parts of the stress tensor $\boldsymbol{\sigma}$, the stress rate tensor $\dot{\boldsymbol{\sigma}}$ and the strain rate tensor $\dot{\boldsymbol{\epsilon}}$ can be expressed respectively as: $\boldsymbol{\sigma}' = \mathscr{D}(\boldsymbol{\sigma})$, $\dot{\boldsymbol{\sigma}}' = \mathscr{D}(\dot{\boldsymbol{\sigma}})$ and $\dot{\boldsymbol{\epsilon}}' = \mathscr{D}(\dot{\boldsymbol{\epsilon}})$.

Since our approach computes pressures in a similar way to standard SPH fluid simulation, we only need to calculate the deviatoric stress rate tensor $\dot{\boldsymbol{\sigma}}'$ and update the deviatoric stress tensor $\boldsymbol{\sigma}'$ at each time step. The mixture deviatoric stress tensor $\boldsymbol{\tau}_{Sm}$ is determined by the deviatoric stress tensor $\boldsymbol{\sigma}'$ and volume fraction of each phase.

We now explain how to compute $\boldsymbol{\sigma}'$ for each of these two material types separately.

4.1 Elastoplastic Materials

When simulating deformable objects in a particle-based method, Müller et al. [2004] used the original position of each particle to calculate the strain tensor. Gerszewski et al. [2009] calculated the deformation gradient tensor to determine the elastic force. Zhou et al. [2013] implemented the elastoplastic framework into an implicit method to achieve stability. However, using the original position of each particle or calculating the deformation gradient tensor differs from how fluids are handled in a multiphase framework. As a particle may contain both fluid and solid phases, the principal component (i.e. pressure) of particle cannot be calculated uniformly if the solid phase is described by the deformation gradient tensor.

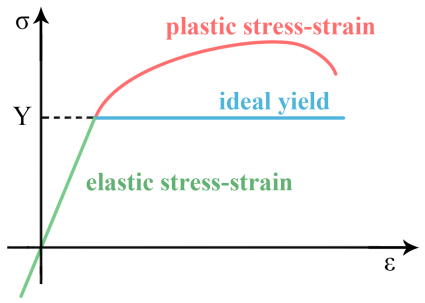

Figure 2: *Yield. When the stress does not reach the yield stress, the material behaves elastically and recovers its original shape when the external force is removed (green). After the stress reaches the yield stress, it changes shape permanently and does not recover (red line). We treat yield in an idealised manner (blue).*

Instead, we use the simple method already used in linear elastic SPH simulation [Libersky and Petschek 1991; Gray et al. 2001], in which the constitutive equation only depends on the velocity gradient.

The velocity gradient $\nabla \boldsymbol{u}$ can be decomposed into a symmetric tensor $\dot{\boldsymbol{\epsilon}}$ and an antisymmetric tensor $\dot{\boldsymbol{\omega}}$:

$$\nabla \boldsymbol{u} = \underbrace{\frac{1}{2}\left(\nabla \boldsymbol{u} + \nabla \boldsymbol{u}^T\right)}_{\dot{\boldsymbol{\epsilon}}} + \underbrace{\frac{1}{2}\left(\nabla \boldsymbol{u} - \nabla \boldsymbol{u}^T\right)}_{\dot{\boldsymbol{\omega}}} \quad (9)$$

where $\dot{\boldsymbol{\omega}}$ is the rotation rate tensor. An elastoplastic material follows a generalized Hooke's law, so:

$$\mathring{\boldsymbol{\sigma}}' = 2G\dot{\boldsymbol{\epsilon}}^{e\prime} \quad (10)$$

where $\dot{\boldsymbol{\epsilon}}^{e\prime}$ is the deviatoric elastic strain rate, G is the shear modulus and $\mathring{\boldsymbol{\sigma}}'$ is the Jaumann derivative of deviatoric stress defined as $\mathring{\boldsymbol{\sigma}}' = \dot{\boldsymbol{\sigma}}' + \boldsymbol{\sigma}' \cdot \dot{\boldsymbol{\omega}} - \dot{\boldsymbol{\omega}} \cdot \boldsymbol{\sigma}'$.

When the material exceeds the yield limit, irreversible plastic deformation occurs. The relationship between strain $\boldsymbol{\epsilon}$ and stress $\boldsymbol{\sigma}$ can be expressed as a curve (see Fig. 2). In our approach, we treat the plastic material as an ideal plastic material in which plastic strain does not change the stress. The total strain rate tensor can thus be expressed as:

$$\dot{\boldsymbol{\epsilon}} = \dot{\boldsymbol{\epsilon}}^e + \dot{\boldsymbol{\epsilon}}^p \quad (11)$$

where $\dot{\boldsymbol{\epsilon}}^p$ is the plastic strain rate tensor. If we substitute Eqn.(11) into Eqn.(10), we obtain:

$$\dot{\boldsymbol{\sigma}}' = \dot{\boldsymbol{\omega}} \cdot \boldsymbol{\sigma}' - \boldsymbol{\sigma}' \cdot \dot{\boldsymbol{\omega}} + 2G(\dot{\boldsymbol{\epsilon}}' - \dot{\boldsymbol{\epsilon}}^{p\prime}). \quad (12)$$

The formulation of $\boldsymbol{\epsilon}^p$ is based on the yield criterion $f(\boldsymbol{\sigma}) = 0$ of the material in which the function $f(\cdot)$ determines the point at which yield begins, and the term $\boldsymbol{\epsilon}^p$ ceases to be zero. For elastoplastic material, we simply use the von Mises criterion to determine yield, so $f(\boldsymbol{\sigma})$ can be expressed as:

$$f(\boldsymbol{\sigma}) = J_2^{(\boldsymbol{\sigma}')} - Y^2$$

where Y is a parameter determining the yield stress, larger Y making the material more resistant to plastic deformation, and $J_2^{(\boldsymbol{\sigma}')}$ is the second principal invariant of deviatoric stress tensor $\boldsymbol{\sigma}'$, given by: $J_2^{(\boldsymbol{\sigma}')} = \frac{1}{2}\boldsymbol{\sigma}' : \boldsymbol{\sigma}'$.

We make use of the von Mises criterion in a similar way to [Solenthaler et al. 2007]: we calculate the deviatoric stress rate tensor using $\mathring{\boldsymbol{\sigma}}' = 2G\dot{\boldsymbol{\epsilon}}'$ and use it to update the deviatoric stress tensor. If the latter satisfies $Y < \sqrt{J_2^{(\boldsymbol{\sigma}')}}$, we simply update $\boldsymbol{\sigma}'$ according to:

$$\boldsymbol{\sigma}' := \boldsymbol{\sigma}'/Y. \tag{13}$$

Further details are given in the Appendix.

Overall, calculation of the deviatoric stress tensor for an elastoplastic material is summarised in Algorithm 2.

Algorithm 2 Elastoplastic constitutive law for deformable bodies

for each particle i **do**
  compute the velocity gradient and strain rate tensor for each particle
  compute the deviatoric stress rate tensor for each particle using $\mathring{\boldsymbol{\sigma}}' = 2G\dot{\boldsymbol{\epsilon}}'$
end for
for each particle i **do**
  update the deviatoric stress tensor for each particle
  if the von Mises yield condition is satisfied **then**
    use Eqn.(13) to correct the deviatoric tensor
  end if
end for

While this approach is not the only one which could be used in our framework, other methods would need to handle the deformation gradient, a tensor whose calculation requires information of the displacement field, and would need to handle interaction with more involved treatment for the volume fraction field.

4.2 Hypoplastic Materials

To simulate granular materials in computer graphics, Bell et al. [2005] used a molecular dynamics model. Zhu and Bridson [2005] treated the spatial domain of sand by decomposing it into two parts. The behaviour of the part near the surface was modelled as shear flows, while the interior was treated as a rigid body. They implemented their approach using a FLIP/PIC framework. However the rigid part of the sand needs to be determined and must move rigidly. This idea is not generally useful in a multiphase framework since the rigid part is treated as a single unit. In SPH simulation, Alduán and Otaduy [2011] used a friction and cohesion model for granular materials based on PCISPH, where shear forces constrain the strain rate. However, PCISPH assumes that the mass and the rest density between particles are uniform which is not valid for multiphase framework [Ren et al. 2014].

Instead, we treat granular materials as hypoplastic materials. The hypoplastic model is well established in engineering as a versatile model for granular materials, and it is based on a strain rate formulation. In this approach, the stress rate $\mathring{\boldsymbol{\sigma}}$ of a material is determined by the current stress tensor $\boldsymbol{\sigma}$ and strain rate $\dot{\boldsymbol{\epsilon}}$. Such models are often used to simulate sands, soils, and clays. In material mechanics, Kolymbas [1991] proposed a simple hypoplastic material constitutive equation which can be expressed as:

$$\mathring{\boldsymbol{\sigma}} = L(\boldsymbol{\sigma}, \dot{\boldsymbol{\epsilon}}) + b(\boldsymbol{\sigma})||\dot{\boldsymbol{\epsilon}}|| \tag{14}$$

where $L(\cdot)$ is a tensor function which is linear in strain rate $\dot{\boldsymbol{\epsilon}}$, similar to that used for an elastoplastic material, b is a linear function of the stress tensor and $||\dot{\boldsymbol{\epsilon}}|| = \sqrt{\dot{\boldsymbol{\epsilon}} : \dot{\boldsymbol{\epsilon}}}$. The first term makes the granular material move rigidly, while the second term is similar to friction in a granular material, controlling how easily the particle glides past each other.

We use the simplified hypoplastic model from [Gudehus 1996; Wu and Bauer 1994], which can be expressed as:

$$\mathring{\sigma} = -c_1 \mathrm{Tr}(\boldsymbol{\sigma})\dot{\boldsymbol{\epsilon}} + c_1 c_2 \frac{\mathrm{Tr}(\boldsymbol{\sigma} \cdot \dot{\boldsymbol{\epsilon}})}{\mathrm{Tr}(\boldsymbol{\sigma})^2}\boldsymbol{\sigma} - c_1 c_3 (\boldsymbol{\sigma} + \boldsymbol{\sigma}')||\dot{\boldsymbol{\epsilon}}|| \tag{15}$$

c_1, c_2 and c_3 are complicated combinations of physical parameters including the tangent modulus, the Poisson ratio, the void ratio, the frictional angle, etc.; see [Gudehus 1996; Wu and Bauer 1994] for more details. Briefly, we may summarise that the factor c_1 is similar to the shear modulus for an elastoplastic material: smaller c_1 makes the granular material more like a shear flow. The factor c_2 is associated with the friction angle: a larger friction angle results from larger c_2. The factor c_3 controls the stiffness: if c_3 is smaller, the internal body of granular material is stiffer.

Simplifying the formulation and substituting $\boldsymbol{\sigma} = -p\boldsymbol{I} + \boldsymbol{\sigma}'$ into Eqn. (15) and rearranging, we get:

$$\mathring{\sigma}' = 3c_1 p\dot{\boldsymbol{\epsilon}}' + c_1 c_2 \left[\frac{\mathrm{Tr}(\boldsymbol{\sigma}' \cdot \dot{\boldsymbol{\epsilon}}) + \mathrm{Tr}(\dot{\boldsymbol{\epsilon}})p}{p^2}\right]\boldsymbol{\sigma}' - 2c_1 c_3 \boldsymbol{\sigma}'||\dot{\boldsymbol{\epsilon}}||. \tag{16}$$

Since the deviatoric stress and pressure are independent, the second term above may vanish at the surface of a granular material if the computed pressure is zero, causing computational problems. We avoid them by changing the second term to $\mathrm{Tr}(\boldsymbol{\sigma} \cdot \dot{\boldsymbol{\epsilon}})/(p^2 + \varepsilon)$ where ε is a constant set to about 1% of the square of the average pressure.

For materials like rock or sands, the pressure is critical in determining yield, and the Drucker-Prager criterion is often used. Following [Narain et al. 2010; Alduán and Otaduy 2011], in this case we make corrections if the deviatoric stress satisfies

$$\alpha_\phi p + k_c < \sqrt{J_2^{(\boldsymbol{\sigma}')}}.$$

The correction is

$$\boldsymbol{\sigma}' := (\alpha_\phi p + k_c)\boldsymbol{\sigma}'/\sqrt{J_2^{(\boldsymbol{\sigma}')}}, \tag{17}$$

as explained in the Appendix; α_ϕ and k_c are coefficients controlling the material's cohesion and internal friction.

Overall, the calculation of the deviatoric stress tensor for hypoplastic materials is given by Algorithm. 3.

5 SPH-based Multiphase Interaction

In this section we describe the method used to combine the solid constitutive equation with the multiphase-flow mixture model. We describe how to calculate the term $\boldsymbol{\tau}_{Sm}$ in Eqn. (8) using the solid deviatoric stress tensor given by Eqn. (10) for an elastoplastic material or Eqn. (16) for a hypoplastic material. We also explain how we modify the SPH interpolation method for the mixture model, allowing us to simply incorporate the solid phases and the multiphase fluid-solid interactions (FSI).

Algorithm 3 Hypoplastic constitutive law for granular materials

for each particle i **do**
  compute the velocity gradient and strain rate tensor for each particle.
  compute the deviatoric stress rate tensor for each particle using Eqn. (16).
end for
for each particle i **do**
  update the deviatoric stress tensor for each particle.
  if the Drucker-Prager yield condition is satisfied **then**
    use Eqn. (17) to correct the deviatoric tensor
  end if
end for

5.1 Discretization

Each particle in a multiphase framework is considered to be a mixture of solids and fluids. We must consider the volume fraction α_k for each phase to calculate the shear tensor $\boldsymbol{\tau}_{S_m}$ for each particle, and changes in shear forces between particles.

We treat each particle in our method in the same way as standard multiphase-fluid SPH particles, with an additional deviatoric stress tensor for each phase, $\boldsymbol{\sigma}'_k$.

Since the constitutive equation in our method only depends on the velocity gradient, we only need to consider how the volume fraction influences the velocity gradient. Ren et al.[2014] took volume fractions into account when discretizing the gradient of an arbitrary tensor term $\boldsymbol{A}$ by simply using an arithmetic average, or average weighted by volume fraction:

$$(\nabla \cdot \boldsymbol{A})_i = \sum_j \frac{m_j}{\rho_j} \sum_k ((\alpha_k)_j \boldsymbol{A}_j \pm (\alpha_k)_i \boldsymbol{A}_i) \cdot \nabla W_{ij}. \quad (18)$$

This assumes that:

$$\sum_j \frac{m_j}{\rho_j} \boldsymbol{A}_i \cdot \nabla W_{ij} = 0,$$

but this formulation does not work well in our framework since the sampling approach of SPH does not always satisfy $\sum_j (m_j/\rho_j)\boldsymbol{u}_i \cdot \nabla W_{ij} = 0$. As $(\alpha_k)_i$ plays an important role in calculating the velocity gradient and the mixture's deviatoric stress tensor force, and since each particle can be a mixture of fluid and solid, Eqn. (18) does not adequately consider the contribution of $(\alpha_k)_i$. Instead, we replace the average in Eqn. (18) by the following expression:

$$(\nabla \cdot \boldsymbol{A})_i = \sum_j \frac{m_j}{\rho_j} \sum_k \Theta\left[(\alpha_k)_i, (\alpha_k)_j\right] (\boldsymbol{A}_j \pm \boldsymbol{A}_i) \cdot \nabla W_{ij} \quad (19)$$

where $\Theta(\cdot,\cdot)$ is an averaging function of its two parameters. We use the harmonic average for two reasons. Firstly, for a particle with a low solids volume fraction, this reduces shear force between particles more effectively. Arithmetic averaging makes the shear force too strong, leading to an unnatural viscosity force between particles even if there are few solid particles nearby. Secondly, the harmonic average also works well for immiscible phases, since averaging ignores those neighbouring particles which have completely different phases from the current particle.

Thus the velocity gradient can be expressed as:

$$\nabla(\boldsymbol{u}_k)_i = \sum_j \frac{m_j}{\rho_j} \frac{2(\alpha_k)_i(\alpha_k)_j}{(\alpha_k)_i + (\alpha_k)_j} \left((\boldsymbol{u}_k)_j - (\boldsymbol{u}_k)_i\right) \nabla W_{ij}. \quad (20)$$

Substituting $\boldsymbol{u}_{mk} = \boldsymbol{u}_k - \boldsymbol{u}_m$ into Eqn. (20), we find that:

$$\nabla(\boldsymbol{u}_k)_i = \sum_j \frac{m_j}{\rho_j} \frac{2(\alpha_k)_i(\alpha_k)_j}{(\alpha_k)_i + (\alpha_k)_j} \times \left((\boldsymbol{u}_{mk})_j - (\boldsymbol{u}_{mk})_i + (\boldsymbol{u}_m)_j - (\boldsymbol{u}_m)_i\right) \nabla W_{ij}. \quad (21)$$

Similarly, the mixture deviatoric tensor term $\boldsymbol{\tau}_{Sm}$ in Eqn. (8) can be expressed as:

$$\boldsymbol{F}_i^{\boldsymbol{\tau}_{Sm}} = m_i \sum_k \sum_j \frac{2(\alpha_k)_i(\alpha_k)_j}{(\alpha_k)_i + (\alpha_k)_j} \left(\frac{(\boldsymbol{\sigma}_k)'_i}{\rho_i^2} + \frac{(\boldsymbol{\sigma}_k)'_j}{\rho_j^2} \right) \cdot \nabla W_{ij}. \quad (22)$$

where $\boldsymbol{F}_i^{\boldsymbol{\tau}_{Sm}}$ is the shear force the surround particles exerting on particle i.

5.2 Dissolution

Our model can easily handle dissolution effects, including soft bodies or granular materials dissolving in a liquid. In our approach, we only consider ideal solutions in which the enthalpy does not change, and the total volume of solvent and solute is unchanged during dissolution. In this case, the volume fraction is the same as the concentration.

The Noyes-Whitney equation can be expressed as:

$$\frac{\mathrm{D}m}{\mathrm{D}t} = \kappa A(C_s - C) \quad (23)$$

where C_s is the saturation concentration, C is the concentration (i.e. volume fraction α in our model), A is the surface area between the dissolving substance and the solvent, and κ is the dissolution coefficient (which depends on temperature). The Noyes-Whitney equation means that the dissolution rate of undissolved solids phases changes is directly proportional to the difference between saturation concentration and the concentration of surrounding dissolved solids phases.

To handle this situation, we replace the third term of Eqn. (5) by the following:

$$\mu_k \left(\frac{\nabla \beta_k}{\beta_k} - \sum_{k'} \frac{\rho_{k'}}{\rho_m} \nabla \beta_{k'} \right)$$

where $\beta_k = \min(\alpha_k, \alpha_s)$ and α_s is the volume saturation concentration corresponding to C_s in Eqn. (23). Note that the volume fraction of an undissolved solid phase is greater than α_s and the volume fraction of a dissolved solid phase is lower than α_s. If the volume fraction of an originally solid particle reaches α_s, the solid component is replaced by fluid. In order to handle this, we change $\Theta(\cdot,\cdot)$ in Eqn. (19) for the dissolving solid phase k to:

$$\Theta((\alpha_k)_i, (\alpha_k)_j) = \begin{cases} 0 & \text{if } (\alpha_k)_i < \alpha_s \text{ or } (\alpha_k)_j < \alpha_s \\ \dfrac{2((\alpha_k)_i - \alpha_s)((\alpha_k)_j - \alpha_s)}{((\alpha_k)_i - \alpha_s) + ((\alpha_k)_j - \alpha_s)} & \text{otherwise} \end{cases} \quad (24)$$

In this way, the solid dissolves when the volume fraction reaches α_s, and the deviatoric stress tensor vanishes automatically. Since the mixture model we use from [Ren et al. 2014] needs volume fraction correction, the volume fraction of solvent fluids may exceed α_s, so we need to label each particle which originally belonged to the solvent. If the volume fraction of the solvent phase k in a fluid particle exceeds α_s, it is corrected to ensure $\alpha_k = \alpha_s$, and the other phases are accordingly normalized.

5.3 Artificial Viscosity of the Mixture

In our method, we use the same artificial viscosity term as in [Becker and Teschner 2007; Akinci et al. 2012; Ren et al. 2014]. We also implement this artificial viscosity at the boundary between immiscible particles and the interior of a solid material; this is essential for elastoplastic material, but optional for hypoplastic material. The pressure force at the interface of a fluid and solid by itself cannot prevent fluid particles from penetrating the solid: only the viscosity force can effectively prevent penetration [Monaghan 1992; Akinci et al. 2012]. For purely solid materials, this force can also improve stability since movements larger than the smooth radius h may occur between solid particles [Bui et al. 2008].

The artificial viscosity takes different forms according to whether the solid and fluid are immiscible or not:

$$\boldsymbol{\Pi}_{ij} = \begin{cases} \gamma_b \pi_{ij} & \text{if immiscible} \\ \frac{1}{2}\sum_k ((\alpha_k)_i + (\alpha_k)_j)\gamma_k \pi_{ij} & \text{otherwise} \end{cases}, \quad (25)$$

where γ_b is the viscosity coefficient at the boundary between the immiscible solid and fluid, and γ_k is the viscosity of each phase: see [Ren et al. 2014]. π_{ij} is defined as:

$$\pi_{ij} = \min(-c_{ij}\phi_{ij}/(\rho_i + \rho_j), 0) \quad (26)$$

where $\phi_{ij} = h\boldsymbol{v}_{ij} \cdot \boldsymbol{x}_{ij}/(|\boldsymbol{x}_{ij}|^2 + \epsilon h^2)$, $\boldsymbol{x}_{ij} = \boldsymbol{x}_i - \boldsymbol{x}_j$, $\boldsymbol{v}_{ij} = \boldsymbol{v}_i - \boldsymbol{v}_j$, and c is the speed of sound in the material. We make the boundary coefficient γ^b larger than the coefficient γ^k of the phases in order to prevent penetration.

5.4 Tensile Instability

SPH simulations suffer from tensile instability for solid simulation, as noted in [Swegle et al. 1995]. We overcome it by using normalized SPH as proposed by [Randles and Libersky 2000] and also used in [Müller et al. 2004]; it is based on moving least squares. We use this method in our multiphase framework by setting the velocity gradient to:

$$\nabla(\boldsymbol{u}_k)_i = (\sum_j \frac{m_j}{\rho_j}\frac{2(\alpha_k)_i(\alpha_k)_j}{(\alpha_k)_i + (\alpha_k)_j}((\boldsymbol{u}_k)_j - (\boldsymbol{u}_k)_i)\boldsymbol{x}_{ij}W_{ij}) \\ (\sum_j \frac{m_j}{\rho_j}\frac{2(\alpha_k)_i(\alpha_k)_j}{(\alpha_k)_i + (\alpha_k)_j}\boldsymbol{x}_{ij}\boldsymbol{x}_{ij}W_{ij})^{-1}. \quad (27)$$

5.5 Implementation

Our implementation uses WCSPH [Becker and Teschner 2007]. It is possible, but requires more effort to integrate our framework with incompressible SPH methods like PCISPH [Solenthaler and Pajarola 2009], IISPH [Ihmsen et al. 2014a] and DFSPH [Bender and Koschier 2015] to handle multiphase fluids: the volume fraction and the density of each particle continually change and the pressure needs to be corrected at each time step.

The proposed multiphase SPH framework can be simply implemented in parallel on a GPU, following Algorithm 4. The blue lines in the algorithm indicate differences from the algorithm in [Ren et al. 2014]. Our unified framework only needs minor changes to additionally deal with miscible and immiscible solids and fluids.

If two phases are miscible but one is not dissolving in the other, e.g. water is being injected into sand, we cannot easily use the mixed particles for rendering. Instead, we use the approach in [Ihmsen et al. 2012] based on refining the solid particles, and determining the fluid content based on the fluid volume fraction of the low resolution particles. This method not only solves this problem, but also enhances the visual effect. In practice, about six times as many refined particles are needed as coarse particles.

Table 1: *Performance for various examples.*

Example	Phases	Particles	Performance
Ex1. Deformable bodies	1	10k	125 steps/s
Ex2. Granular materials	1	70k	23 steps/s
Ex3. Multiphase FSI	3	110k	16 steps/s
Ex4. Water in sand	2	140k–170k	15–12 steps/s
Ex5. Dissolved ball	2	70k–100k	18–15 steps/s
Ex6. Dissolved granular	3	110k–250k	12–6 steps/s
Ex7. Coffee-candy	3	110k–250k	12–6 steps/s

Algorithm 4 GPU implementation for the multiphase SPH framework

repeat
  for each particle i **do**
    compute the density and the pressure for each particle using standard SPH
  end for
  for each particle i **do**
    compute the drift velocity using Eqn. (5), then compute the diffusion tensor and correct α using Eqn. (6) and Eqn. (7)
  end for
  for each particle i **do**
    compute its velocity gradient using Eqn. (21)
    use Algorithms 2 and 3 to update the deviatoric stress tensor for each phase
  end for
  for each particle i **do**
    for each neighbouring particle j **do**
      compute the force F_{ij}^p as in standard SPH
      compute the force F^{rSm} according to Eqn. (22)
      compute the viscosity force according to Eqn. (25)
      sum these forces to give the total force acting on the particle
    end for
  end for
  for each particle i **do**
    advance the particle
  end for
  $t \leftarrow t + \Delta t$
until end of simulation

6 Results

We have implemented the above approach on an NVIDIA GeForce GTX980 16GB GPU. The time step is set between 10^{-3} and 10^{-4}; a leapfrog approach is used to prevent penetration and to ensure convergence of $\boldsymbol{\epsilon}'$, following the approach in [Ren et al. 2014]. Table 1 records the performance of our multiphae SPH framework for the various examples shown here.

Example 1 (see Fig. 3) demonstrates two elastoplastic blocks dropping onto a table. Their shear modulus is $G = 10^5$ Pa. The yield stress is set as $Y = 10^4$ Pa for the block on the left to simulate elastic deformation, and $Y = 45$ Pa for the block on the right to simulate plastic deformation. We calculate the deviatoric stress tensor of the elastoplastic material, and use the state equation to calculate the pressure. The left block with large yield stress bounces

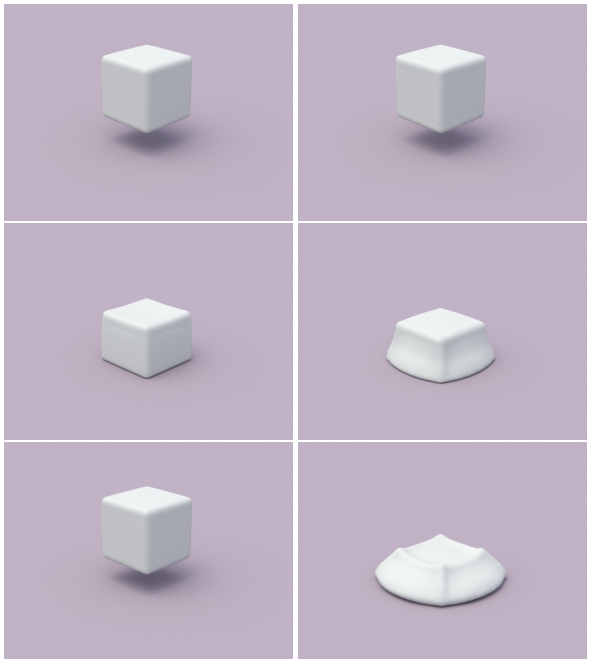

Figure 3: *An elastic block and a plastic block drop onto a table. The elastic block on the left bounces back up and recovers its shape. The plastic block on the right deforms permanently.*

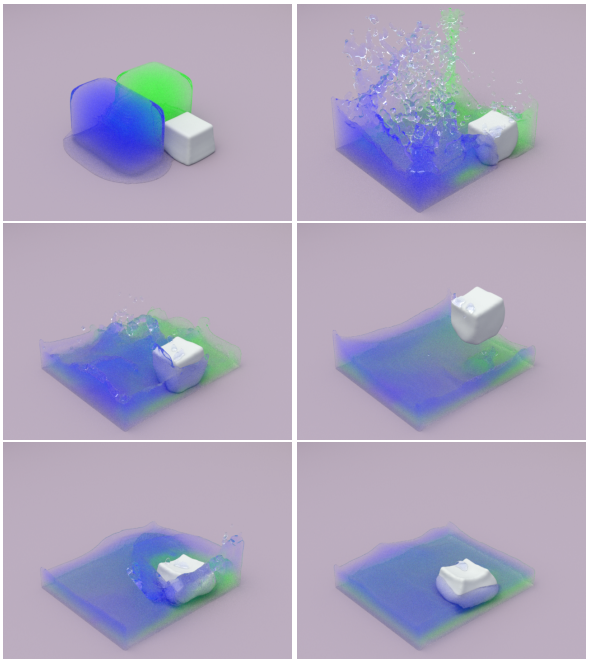

Figure 4: *From left to right, top to bottom: an elastoplastic block interacting with two fluids*

Table 2: *Hypoplastic parameters for simulation shown in Fig. 5*

Column	c_1	c_2	c_3
1	700	0	0.5
2	30	0	0.5
3	700	1	0.5
4	700	0	0

after hitting the table, changing shape before it bounces, and finally returns to its original shape as it rises. The right block with low yield stress deforms permanently and does not return to its original shape.

In Example 2 (see Fig. 5) , using our approach for hypoplasticity, we start with an unstable block of granular material in the initial frame. Fig. 5 shows how the block collapses due to gravity. With different parameter settings, we can obtain different behaviour in the granular material. The detailed parameter setting is listed in Table 2. Smaller c_1 results in greater shear flow; larger c_2 increases the friction angle; and smaller c_3 makes the body of the granular material more rigid.

Example 3 (see Fig. 4) shows how multiphase fluid-solid coupling can be simply handled by our approach. A dam break occurs between two fluids, and the fluid mixture interacts with an elastoplastic block. The density ratio between the solid block, the blue fluid and the green fluid is $2:1:3$; all phases are immiscible with each other. As the liquids scour the block, the block changes shape. We then raise the block and drop it back into the liquid. The block becomes flattened by the end. The artificial viscosity term given in Section 5.3 prevents penetration of fluid into the solid body.

Example 4 (see Fig. 6) demonstrates flow in a porous medium. Water is poured onto sand, permeating the sand and wetting it. By the end, the water has created a large hole in the middle of the sand, which collapses due to decrease in the deviatoric stress tensor. The sand and fluid phases are miscible. Unlike the results given in [Lenaerts and Dutr 2009], which are based on porous flow, ours are based on our multiphase framework. The density of sand:water is $2:1$; and the hypoelastic parameters c_1, c_2 and c_3 are set as $700:1:0.5$, respectively.

Example 5 (Fig. 7) demonstrates a dissolution process: an elastoplastic ball is dropped into a square glass box and then water is poured over it. The ball dissolves in the water, making it change color. The density ratio of ball:water is $2:1$, and $\alpha_s = 0.5$.

In Example 6 (see Fig. 8), a volume of granular material are dropped into a box which holds an elastoplastic ball, the grains pile over the ball after which water is poured into the box, dissolving the granular material to form a colourless liquid. The ball is immiscible in the water while the granular material dissolves. The density ratio for ball:granular material:water is $2:1:1$; $\alpha_s = 0.5$.

Example 7 (see Fig. 1) shows instant coffee granules and a soft candy dissolving in water. As water is poured into the glass container, the contents on the left side become more viscous due to saturation. After stirring, all solids are dissolved. The density ratio of candy:coffee:water is 2:1:1 and α_s is 0.5.

7 Discussion and Future Work

We have given a unified framework which extends the multiphase-fluid SPH framework to also handle deformable bodies and granular materials. Through the extended multiphas SPH framework, we have also demonstrated a new approach to model fluid-solid interaction, especially for multiphase fluids and solids. Our framework is simple and is able to simulate a wide variety of phenomena including multiple interactive fluids and solids, mixtures with granular materials, and dissolution effects, as the above experiments show.

Our method uses a linear elastic model, since it is simple and does not need to consider the initial shape. We only need to use the velocity gradient to calculate ϵ. This approach can be incorporated

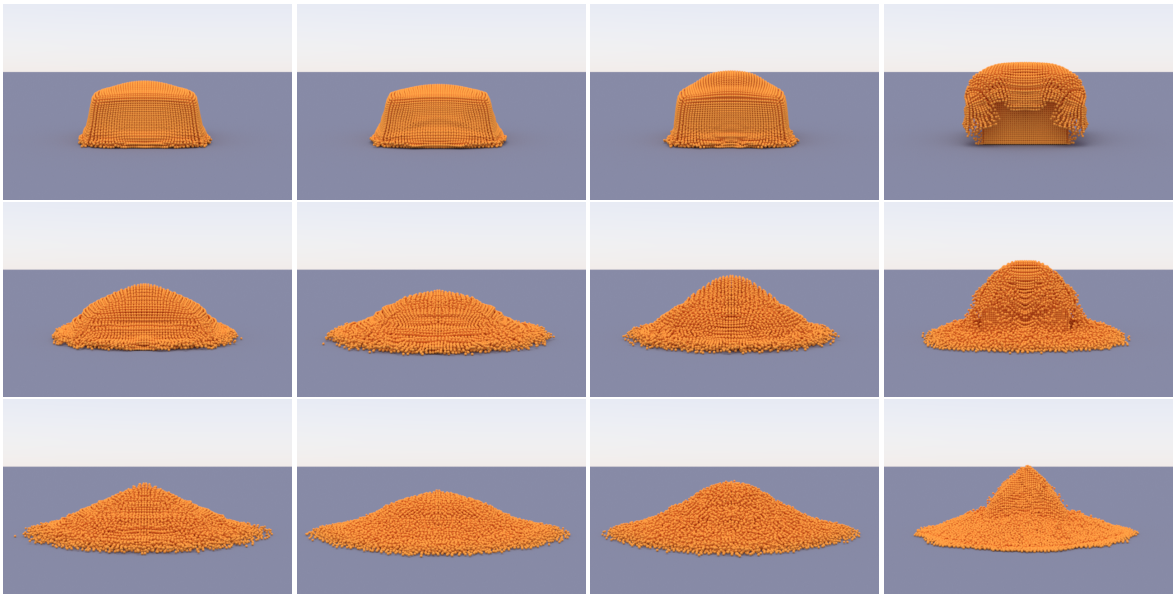

Figure 5: *Granular material modelled by the hypoplastic constitutive law. Left: base case. Mid-left: smaller c_1 leads to greater shear flow. Mid-right: larger c_2 increases the friction angle. Right: smaller c_3 makes the core of the granular material more rigid.*

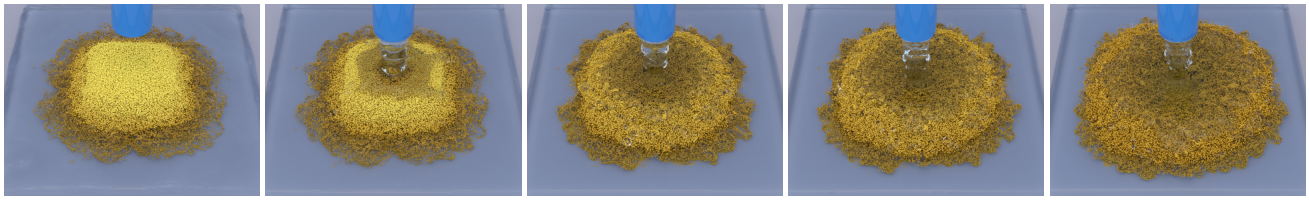

Figure 6: *Water poured onto a sand pile, permeating the sand and wetting it. The water makes a large hole in the middle of the sand, which collapses due to decrease in the deviatoric stress tensor.*

into the mixture model simply without considering the deformation gradient change for each different component. However, it is less than ideal for purely elastic materials which experience large deformations, since computing the velocity gradient only cannot take this into account. As a result, the current scheme cannot model large elastic deformation due to accuracy loss from reference shape drift and nonlinear elastic materials cannot be modeled. It would be an interesting and challenging future work to take into account the information of the deformation gradient tensor and consider more versatile elastic and plastic material models (e.g. [Jones et al. 2014; Martin et al. 2010]), while maintaining the uniformity and simplicity of the simulation framework.

As granular materials are represented in our framework by the volume fraction field, we cannot directly render granular particles when they mix with fluids, and need to perform a post-processing refinement [Ihmsen et al. 2012] for rendering. Alternatively, besides the volume/mass fraction of the particle phase, it could be beneficial to incorporate the number density and size distribution of particles into the simulation. But this is likely to require significant research effort.

The proposed multiphase SPH framework is able to simulate multiple fluids, elastoplastic bodies and granular materials and their interactions including flow in porous media and dissolution of deformable solids. Despite the relatively wide range of fluid-solid phenomena that are captured by the proposed framework, there remains a wider range of interesting phenomena that require further investigation, such as gas-liquid-solid phase transition and viscoelastic materials (e.g. snow) etc. Along this line, we do not aim for a single approach that works best for all applications, and instead we look for a simple and uniform strategy that is also versatile and efficient.

Appendix: von Mises and Drucker-Prager criteria

In material mechanics, when the stress of an elastoplastic material reaches the yield criterion $f(\boldsymbol{\sigma}) = 0$, the material begins to yield and no longer returns to the original shape. For example, the von Mises criterion states that when the distortion energy $dE_Q = \boldsymbol{\sigma}' : d\boldsymbol{\epsilon}'$ exceeds a certain value, the material begin to yield. For an ideal material, after the material starts yielding, the stress no longer depends on the strain. Fig. 2 demonstrate the yield process for an elastoplastic material. The green line is the region of elastic deformation, the red line shows actual plastic yield for a real material, and the blue line is the idealized plastic yield curve. Several yield criteria can be used for $f(\boldsymbol{\sigma})$. The von Mises criterion is $f(\boldsymbol{\sigma}) = \sqrt{J_2^{(\boldsymbol{\sigma}')}} - Y^2$, while the Drucker-Prager yield criterion is $f(\boldsymbol{\sigma}) = \sqrt{J_2^{(\boldsymbol{\sigma}')}} + \alpha_\phi p - k_c = 0$ with

$$\alpha_\phi = \frac{tg\phi}{\sqrt{9 + 12tg^2\phi}}, \qquad k_c = \frac{3c}{\sqrt{9 + 12tg^2\phi}},$$

where c is the cohesion coefficient and ϕ is the internal friction.

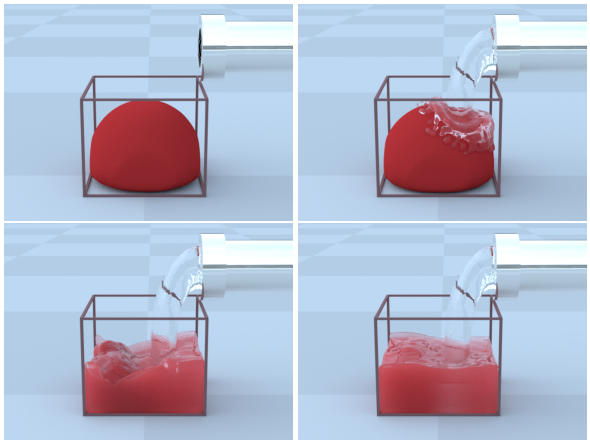

Figure 7: *An elastoplastic ball dropped into a square glass box, with water poured over it. The ball dissolves in the water, making the water change color.*

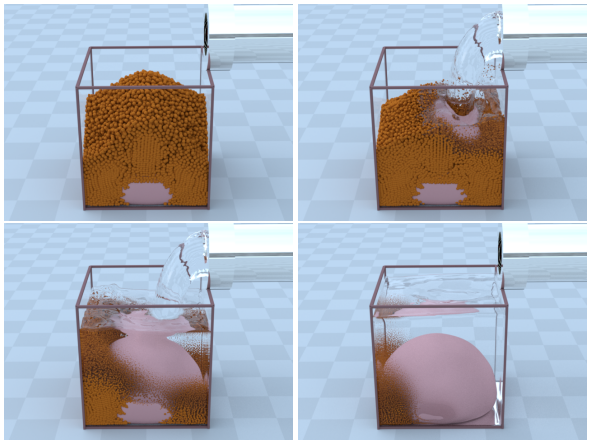

Figure 8: *A volume of granular material are dropped into a box on top of an elastoplastic ball, and then water is poured in, dissolving the granular material to give a colourless liquid.*

In our framework, the von Mises criterion can be applied in conjunction with normalisation by Eqn.(13). The Drucker-Prager criterion can be expressed as [Bui et al. 2008]:

$$\dot{\boldsymbol{\epsilon}}^p = \lambda \left(3\alpha_\phi K \boldsymbol{I} + \frac{G}{\sqrt{J_2}} \boldsymbol{\sigma} \right) \tag{28}$$

where $J_2 = \frac{1}{2}\boldsymbol{\sigma} : \boldsymbol{\sigma}$ is the second principal invariant of stress tensor $\boldsymbol{\sigma}$, λ is the drift coefficient, and K is the bulk modulus. However, this will change the pressure in the material. Thus, instead, we use a simplified method: if the deviatoric stress satisfies $\alpha_\phi p + k_c < \sqrt{J_2}$, we set:

$$\boldsymbol{\sigma}' := \frac{(\alpha_\phi p + k_c)\boldsymbol{\sigma}'}{\sqrt{J_2}} \tag{29}$$

which is the same form as in [Alduán and Otaduy 2011].

Acknowledgements

The authors would like to thank the anonymous reviewers for their thoughtful comments. This work is supported by the Natural Science Foundation of China (Project Number 61120106007, 61521002), Research Grant of Beijing Higher Institution Engineering Research Center, Tsinghua University Initiative Scientific Research Program, and the Royal Academy of Engineering and the Leverhulme Trust (Project Number LSRF1415/11/96).

References

AKINCI, N., IHMSEN, M., AKINCI, G., SOLENTHALER, B., AND TESCHNER, M. 2012. Versatile rigid-fluid coupling for incompressible sph. *ACM Trans. Graph. 31*, 4 (July), 62:1–62:8.

AKINCI, N., CORNELIS, J., AKINCI, G., AND TESCHNER, M. 2013. Coupling elastic solids with sph fluids. *Journal of Computer Animation and Virtual Worlds*.

ALDUÁN, I., AND OTADUY, M. A. 2011. Sph granular flow with friction and cohesion. *Proceedings of the 2011 ACM SIGGRAPH/Eurographics Symposium on Computer Animation*, 25–32.

BAUER, E. 1996. Calibration of a comprehensive hypoplastic model for granular materials. *Soils and Foundations 36*, 1, 13–26.

BECKER, M., AND TESCHNER, M. 2007. Weakly compressible sph for free surface flows. *Proceedings of the 2007 ACM SIGGRAPH/Eurographics Symposium on Computer Animation*, 209–217.

BECKER, M., IHMSEN, M., AND TESCHNER, M. 2009. Corotated sph for deformable solids. *Proceedings of the Fifth Eurographics Conference on Natural Phenomena*, 27–34.

BELL, N., YU, Y., AND MUCHA, P. J. 2005. Particle-based simulation of granular materials. *Proceedings of the 2005 ACM SIGGRAPH/Eurographics Symposium on Computer Animation*, 77–86.

BENDER, J., AND KOSCHIER, D. 2015. Divergence-free smoothed particle hydrodynamics. *SCA '15*, 147–155.

BUI, H. H., FUKAGAWA, R., SAKO, K., AND OHNO, S. 2008. Lagrangian meshfree particles method (sph) for large deformation and failure flows of geomaterial using elasticcplastic soil constitutive model. *International Journal for Numerical and Analytical Methods in Geomechanics 32*, 12, 1537–1570.

GERSZEWSKI, D., BHATTACHARYA, H., AND BARGTEIL, A. W. 2009. A point-based method for animating elastoplastic solids. *Proceedings of the 2009 ACM SIGGRAPH/Eurographics Symposium on Computer Animation*, 133–138.

GRAY, J., MONAGHAN, J., AND SWIFT, R. 2001. SPH elastic dynamics. *Computer Methods in Applied Mechanics and Engineering 190*, 49C50, 6641 – 6662.

GUDEHUS, G. 1996. A comprehensive constitutive equation for granular materials. *Soils and Foundations 36*, 1, 1–12.

HILL, R. 1998. *The Mathematical Theory of Plasticity.* Oxford, Clarendon Press.

IHMSEN, M., WAHL, A., AND TESCHNER, M. 2012. High-resolution simulation of granular material with sph. *VRIPHYS*, 53–60.

IHMSEN, M., CORNELIS, J., SOLENTHALER, B., HORVATH, C., AND TESCHNER, M. 2014. Implicit incompressible sph. *IEEE Transactions on Visualization and Computer Graphics 20*, 3 (Mar.), 426–435.

IHMSEN, M., ORTHMANN, J., SOLENTHALER, B., KOLB, A., AND TESCHNER, M. 2014. SPH Fluids in Computer Graphics. *Eurographics 2014 - State of the Art Reports*.

JONES, B., WARD, S., JALLEPALLI, A., PERENIA, J., AND BARGTEIL, A. W. 2014. Deformation embedding for point-based elastoplastic simulation. *ACM Trans. Graph. 33*, 2 (Apr.), 21:1–21:9.

KEISER, R., ADAMS, B., GASSER, D., BAZZI, P., DUTRÉ, P., AND GROSS, M. 2005. A unified lagrangian approach to solid-fluid animation. *Proceedings of the Second Eurographics / IEEE VGTC Conference on Point-Based Graphics*, 125–133.

KOLYMBAS, D. 1991. Computer-aided design of constitutive laws. *International Journal for Numerical and Analytical Methods in Geomechanics 15*, 8, 593–604.

LENAERTS, T., AND DUTR, P. 2009. Mixing fluids and granular materials. *Computer Graphics Forum 28*, 2, 213–218.

LENAERTS, T., ADAMS, B., AND DUTRÉ, P. 2008. Porous flow in particle-based fluid simulations. *ACM Trans. Graph. 27*, 3 (Aug.), 49:1–49:8.

LIBERSKY, L., AND PETSCHEK, A. 1991. Smooth particle hydrodynamics with strength of materials. In *Advances in the Free-Lagrange Method Including Contributions on Adaptive Gridding and the Smooth Particle Hydrodynamics Method*, H. Trease, M. Fritts, and W. Crowley, Eds., vol. 395 of *Lecture Notes in Physics*. Springer Berlin Heidelberg, 248–257.

MACKLIN, M., AND MÜLLER, M. 2013. Position based fluids. *ACM Trans. Graph. 32*, 4 (July), 104:1–104:12.

MACKLIN, M., MÜLLER, M., CHENTANEZ, N., AND KIM, T.-Y. 2014. Unified particle physics for real-time applications. *ACM Trans. Graph. 33*, 4 (July), 153:1–153:12.

MANNINEN, M., TAIVASSALO, V., AND KALLIO, S. 1996. On the mixture model for multiphase flow. *VTT Technical Research Centre of Finland*, 288.

MARTIN, S., KAUFMANN, P., BOTSCH, M., GRINSPUN, E., AND GROSS, M. 2010. Unified simulation of elastic rods, shells, and solids. *ACM Trans. Graph. 29*, 4 (July), 39:1–39:10.

MONAGHAN, J. J. 1992. Smoothed particle hydrodynamics. *Annual Review of Astronomy and Astrophysics 30*, 1, 543–574.

MONAGHAN, J. 1997. Sph and riemann solvers. *J. Comput. Phys. 136*, 2 (Sept.), 298–307.

MÜLLER, M., AND CHENTANEZ, N. 2011. Solid simulation with oriented particles. *ACM Trans. Graph. 30*, 4 (July), 92:1–92:10.

MÜLLER, M., CHARYPAR, D., AND GROSS, M. 2003. Particle-based fluid simulation for interactive applications. *Proceedings of the 2003 ACM SIGGRAPH/Eurographics Symposium on Computer Animation*, 154–159.

MÜLLER, M., KEISER, R., NEALEN, A., PAULY, M., GROSS, M., AND ALEXA, M. 2004. Point based animation of elastic, plastic and melting objects. *Proceedings of the 2004 ACM SIGGRAPH/Eurographics Symposium on Computer Animation*, 141–151.

MÜLLER, M., HEIDELBERGER, B., TESCHNER, M., AND GROSS, M. 2005. Meshless deformations based on shape matching. *ACM SIGGRAPH 2005 Papers*, 471–478.

MÜLLER, M., SOLENTHALER, B., KEISER, R., AND GROSS, M. 2005. Particle-based fluid-fluid interaction. *Proceedings of the 2005 ACM SIGGRAPH/Eurographics Symposium on Computer Animation*, 237–244.

NARAIN, R., GOLAS, A., AND LIN, M. C. 2010. Free-flowing granular materials with two-way solid coupling. *ACM SIGGRAPH Asia 2010 Papers*, 173:1–173:10.

PEER, A., IHMSEN, M., CORNELIS, J., AND TESCHNER, M. 2015. An implicit viscosity formulation for sph fluids. *ACM Trans. Graph. 34*, 4 (July), 114:1–114:10.

RANDLES, P. W., AND LIBERSKY, L. D. 2000. Normalized sph with stress points. *International Journal for Numerical Methods in Engineering 48*, 10, 1445–1462.

REN, B., LI, C., YAN, X., LIN, M. C., BONET, J., AND HU, S.-M. 2014. Multiple-fluid sph simulation using a mixture model. *ACM Trans. Graph. 33*, 5 (Sept.), 171:1–171:11.

SCHAEFFER, D. G. 1987. Instability in the evolution equations describing incompressible granular flow. *Journal of Differential Equations 66*, 1, 19 – 50.

SHAO, X., ZHOU, Z., MAGNENAT-THALMANN, N., AND WU, W. 2015. Stable and fast fluid-solid coupling for incompressible sph. *Comput. Graph. Forum 34*, 1 (Feb.), 191–204.

SOLENTHALER, B., AND PAJAROLA, R. 2008. Density contrast sph interfaces. *SCA '08*, 211–218.

SOLENTHALER, B., AND PAJAROLA, R. 2009. Predictive-corrective incompressible sph. *ACM Trans. Graph. 28*, 3 (July), 40:1–40:6.

SOLENTHALER, B., SCHLÄFLI, J., AND PAJAROLA, R. 2007. A unified particle model for fluid-solid interactions. *Comput. Animat. Virtual Worlds 18*, 1 (Feb.), 69–82.

STOMAKHIN, A., SCHROEDER, C., CHAI, L., TERAN, J., AND SELLE, A. 2013. A material point method for snow simulation. *ACM Trans. Graph. 32*, 4 (July), 102:1–102:10.

STOMAKHIN, A., SCHROEDER, C., JIANG, C., CHAI, L., TERAN, J., AND SELLE, A. 2014. Augmented mpm for phase-change and varied materials. *ACM Trans. Graph. 33*, 4 (July), 138:1–138:11.

SULSKY, D., CHEN, Z., AND SCHREYER, H. 1994. A particle method for history-dependent materials. *Computer Methods in Applied Mechanics and Engineering 118*, 1C2, 179 – 196.

SWEGLE, J., HICKS, D., AND ATTAWAY, S. 1995. Smoothed particle hydrodynamics stability analysis. *Journal of Computational Physics 116*, 1, 123 – 134.

TAKAHASHI, T., DOBASHI, Y., FUJISHIRO, I., NISHITA, T., AND LIN, M. C. 2015. Implicit formulation for sph-based viscous fluids. *Comput. Graph. Forum 34*, 2, 493–502.

WU, W., AND BAUER, E. 1994. A simple hypoplastic constitutive model for sand. *International Journal for Numerical and Analytical Methods in Geomechanics 18*, 12, 833–862.

YANG, T., CHANG, J., REN, B., LIN, M. C., ZHANG, J. J., AND HU, S.-M. 2015. Fast multiple-fluid simulation using helmholtz free energy. *ACM Trans. Graph. 34*, 6 (Oct.), 201:1–201:11.

ZHOU, Y., LUN, Z., KALOGERAKIS, E., AND WANG, R. 2013. Implicit integration for particle-based simulation of elasto-plastic solids. *Computer Graphics Forum 32*, 7, 215–223.

ZHU, Y., AND BRIDSON, R. 2005. Animating sand as a fluid. *ACM SIGGRAPH 2005 Papers*, 965–972.